Observation of the metallic mosaic phase in 1*T*-TaS_2 at equilibrium

Björn Salzmann,[1,*] Elina Hujala,[1,2] Catherine Witteveen,[3,4] Baptiste Hildebrand,[1] Helmuth Berger,[5] Fabian O. von Rohr,[3,4] Christopher W. Nicholson,[1,6] and Claude Monney[1]

[1]*Département de Physique and Fribourg Center for Nanomaterials, Université de Fribourg, CH-1700 Fribourg, Switzerland*
[2]*Lappeenranta-Lahti University of Technology LUT, FI-53850 Lappeenranta, Finland*
[3]*Department of Chemistry, University of Zurich, CH-8057 Zürich, Switzerland*
[4]*Department of Quantum Matter Physics, University of Geneva, CH-1211 Geneva, Switzerland*
[5]*Institut de Physique des Nanostructures, École Polytechnique Fédérale de Lausanne (EPFL), CH-1015 Lausanne, Switzerland*
[6]*Fritz Haber Institute of the Max Planck Society, D-14195 Berlin, Germany*

(Received 13 January 2023; revised 28 April 2023; accepted 18 May 2023; published 14 June 2023)

The transition-metal dichalcogenide tantalum disulphide (1*T*-TaS_2) hosts a commensurate charge density wave (CCDW) at temperatures below 165 K where it also becomes insulating. The low temperature CCDW phase can be driven into a metastable "mosaic" phase by means of either laser or voltage pulses, which shows a large density of CDW domain walls as well as a closing of the electronic band gap. The exact origins of this pulse-induced metallic mosaic are not yet fully understood. Here, using scanning tunneling microscopy and spectroscopy (STM/STS), we observe the occurrence of such a metallic mosaic phase on the surface of TaS_2 without prior pulse excitation over continuous areas larger than $100 \times 100\,\mathrm{nm}^2$ and macroscopic areas on the millimeter scale. We attribute the appearance of the mosaic phase to the presence of surface defects which cause the formation of the characteristic dense domain wall network. Based on our STM measurements, we further argue how the appearance of the metallic behavior in the mosaic phase could be explained by local stacking differences of the top layer. Thus we provide a potential avenue to explain the origin of the pulse-induced mosaic phase.

DOI: 10.1103/PhysRevMaterials.7.064005

I. INTRODUCTION

Quasi-two-dimensional (2D) materials present a wide range of interesting physical phenomena and promising technological applications [1–5]. One class of such materials are transition-metal dichalcogenides (TMDCs), which generally have a layered structure. However, despite this structure, changes to their interlayer interactions can strongly influence their electronic properties [6–10]. One such material for which the influence of interlayer stacking has recently been shown to be of great relevance to the electronic properties is 1*T*-TaS_2. The 1*T* polytype of TaS_2 exists in a near commensurate charge density wave (CDW) state at room temperature with 13 Ta atoms forming a so-called star of David (SOD) pattern within the layers of the TaS_2 structure [11]. Upon cooling, a phase transition to a fully commensurate CDW phase with a periodicity of $\sqrt{13} \times \sqrt{13}$ occurs at around 165 K, accompanied by a transition from metallic to insulating behavior [12]. An illustration of the atomic structure of TaS_2 can be found in the upper panel of Fig. 1(a) and the in-plane CDW structure in the lower panel. Unexpectedly, it was previously found that a so-called mosaic or hidden phase can be accessed from the commensurate charge density wave (CCDW) phase of TaS_2 by applying either single laser [13,14] or voltage pulses [15–18]. On the microscopic scale, this phase is characterized by an increased density of domain walls at the site of the pulse from which its name derives. Interestingly, within the region of these dense domain walls, the sample surface becomes metallic. A drop in macroscopic resistivity can be observed accordingly. The appearance of metallic behavior in the normally insulating CCDW phase outside the mosaic phase has also been attributed to changes in the SOD stacking order [19,20]. SODs can stack on top of each other in three distinct ways, as determined by the location of their center atom with respect to the other SOD: with both center atoms directly on top of each other, with the top center atom atop one of the inner six atoms of the lower SOD which are indicated in blue in the bottom panel of Fig. 1(a) and with the top center atom atop one of the outer six atoms, indicated in green in Fig. 1(a). In the following, we will adopt the nomenclature used in Ref. [19] and refer to these three stacking orders as AA, AB, and AC stacking, respectively. Previous investigations have determined that the bulk stacking order consists of pairs of AA stacked layers which are in turn AC stacked [20–25]. Both AA and AC stacked layers are insulating, albeit with different origins for this insulating behavior [19,24–27]. On the other hand, AB stacked layers have been reported to sometimes be metallic [19], presenting a potential explanation for the metallic behavior of the mosaic phase. However, the exact cause for the formation of the mosaic phase has so far not been established.

Here, we present scanning tunneling microscopy (STM) and scanning tunneling spectroscopy (STS) measurements of a mosaic phase occurring on an untreated surface, that is, a surface not exposed to external stimulation. As in the pulse-induced mosaic, we also observe a closing of the electronic gap within specific domains of this mosaic phase. However,

*bjoern.salzmann@unifr.ch

 ©2023 American Physical Society

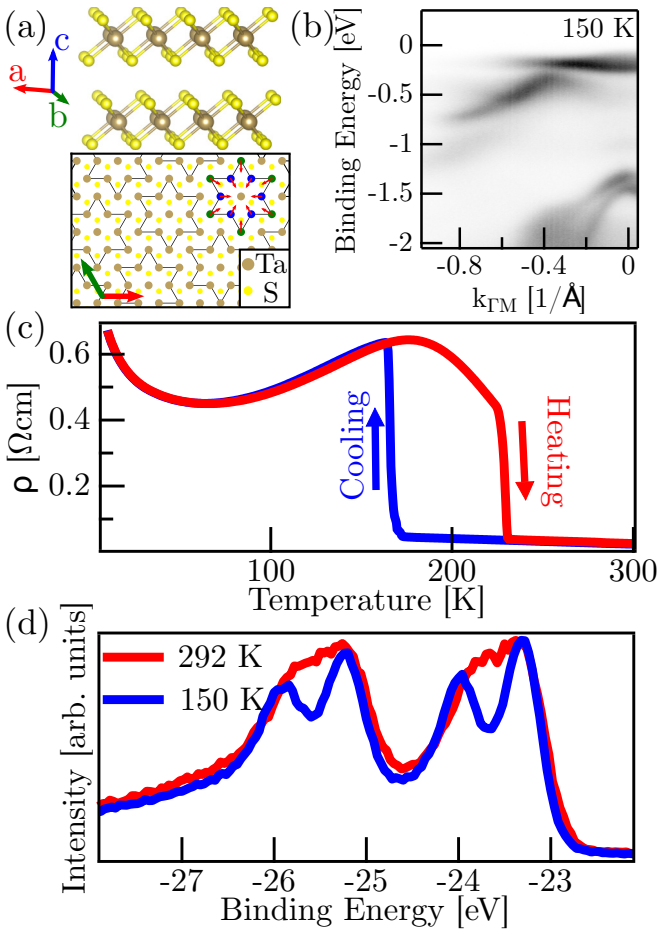

FIG. 1. (a) Top panel shows the atomic structure of TaS_2 including two layers stacked along the c axis. The bottom panel is a view of the surface in the a-b plane of the material with only top layer atoms included. The SOD structure of the CDW is displayed in black across the image with the movement of the Ta atoms indicated by red arrows for one SOD. (b) ARPES image taken at a photon energy of 21.2 eV at 150 K. The band structure is typical for the CCDW phase. (c) Resistivity as a function of temperature measured on a TaS_2 sample of the same batch as the one used for other measurements in this study. The transition from the near-commensurate to the commensurate CDW phase occurs around 165 K during cooling as expected for $1T$-TaS_2. (d) XPS measurements of a TaS_2 sample at different temperatures containing the Ta $4f$ peaks. The peak positions correspond to those expected from the $1T$ polytype.

the spatial extent of the mosaic phase in our measurements is significantly larger than that of the ones induced by local stimulation and can be found across distances on the order of millimeters on the sample surface. Based on our measurements and previous theoretical [28] and experimental work on Ti doped TaS_2 [29], we suggest that the formation of the mosaic phase in our samples is caused by a high density of charged surface defects which lead to the formation of domain walls. Through analysis of the shift between different CDW domains, we find supporting evidence that these domain walls in turn locally alter the stacking order of the top layer of the material, causing it to turn metallic. Thus we both explain the occurrence of a metallic mosaic in our samples and provide experimental evidence for a possible origin of the pulse-induced mosaic.

II. METHODS

High quality single crystals of $1T$-TaS_2 were grown by the chemical vapor transport (CVT) method using $TaCl_5$ as a transport agent. First, polycrystalline samples of $1T$-TaS_2 were synthesized by mixing stoichiometric amounts of tantalum (powder, Alfa Aesar, 99.99%) and sulfur (pieces, Alfa Aesar, 99.999%) of a total mass of 1 g. The reactants were sealed in a quartz ampoule ($l = 9$ cm, $o_i = 9$ mm) under 1/3 atm of argon. The quartz ampoule was heated to 1000 °C at a rate of 180 °C/h, kept at this temperature for 4 days and subsequently quenched in water. In a second step, 200 mg of the as synthesized powder and 10 mg $TaCl_5$ (anhydrous, powder, VWR, 99.999%) were sealed in a quartz ampoule ($l = 20$ cm, $o_i = 7$ mm) under vacuum and heated for 6 days in a two zone furnace in which the source zone and the growth zone temperatures were fixed at 980 °C and 850 °C, respectively. Eventually, the tube was quenched in cold water to ensure the retaining of the $1T$ phase. The product was confirmed to be phase pure by powder x-ray diffraction. Patterns were collected on an STOE STADI P diffractometer in transmission mode equipped with a Ge-monochromator using Cu $K_{\alpha 1}$ radiation and on a Rigaku SmartLab in reflection mode using Cu K_α radiation.

STM measurements were taken using a commercial low temperature STM system (Scienta Omicron) at 4.5 K at a pressure of $\leqslant 5 \times 10^{-11}$ mbar using the constant current method with a current of 0.1 nA unless otherwise noted. STS measurements were carried out using a lock-in technique with a frequency of 955 Hz. Samples were cleaved using scotch tape at room temperature at a pressure of $\leqslant 5 \times 10^{-8}$ mbar before being transferred to the already cold STM or other measurement chambers. Angle resolved photoemission spectroscopy (ARPES) measurements were obtained with the 21.2 eV photon energy He I spectral line produced by a commercial UV lamp (Specs GmbH) and a commercial hemispherical electron analyzer (Scienta Omicron). X-ray photoemission spectroscopy (XPS) measurements were performed using a photon energy of 1486.6 eV, produced from monochromatized Al K_α emission (Specs GmbH). Samples which showed the mosaic phase in STM measurements generally did not undergo other prior measurements.

III. RESULTS

To verify that our samples do not show any macroscopic differences to previously studied $1T$-TaS_2 samples and that our findings are therefore generally applicable to $1T$-TaS_2 samples, we have performed several characterization measurements, the results of which are presented in Figs. 1(b)–1(d). Figure 1(b) shows a representative ARPES image obtained with a photon energy of 21.2 eV at a temperature of 150 K, along the $\bar{\Gamma}\bar{M}$ direction of the surface Brioullin zone. The dispersion is in good agreement with previous ARPES measurements of $1T$-TaS_2 in the CCDW phase [27,30,31]. Figure 1(c) presents resistivity as a function of temperature. The jump in resistivity occurs at the near

commensurate to commensurate phase transition at around 165 K upon cooling as expected from previous studies [27,32] and agrees with observations from temperature dependent ARPES measurements in which we find a similar transition temperature. Figure 1(d) displays XPS spectra of the Ta $4f$ core levels at room temperature and 150 K, i.e., above and below the CCDW phase transition temperature. The two peak structure is expected due to the CDW creating two inequivalent Ta sites on the outer and inner ring of the SOD structure [33]. The enhanced peak splitting observed below the CCDW transition temperature is ascribed to a stronger CDW amplitude after the transition [33]. Overall, these findings are in agreement with previous XPS measurements [33,34]. Additional characterization measurements can be found in the Supplemental Material [35] (see also Refs. [36–39] therein) and also show no unusual behavior. In summary, we find that our samples macroscopically behave as expected from previous literature using the above characterization techniques.

Figure 2(a) shows an STM image of the surface of TaS_2 taken with a gap voltage of −0.4 V. The inset presents a magnified section of the main image, indicated by the dashed square. In both the main image and the inset, the bright spots forming the periodic lattice correspond to individual SODs in the CDW phase and not to individual surface atoms. The appearance of the surface is as expected from previous observations on $1T$-TaS_2 in the CCDW phase with the SODs aligned in a hexagonal lattice. However, our images contain an increased number of dark defect sites as compared to literature which we will discuss later. In contrast, Fig. 2(b) is another image of the TaS_2 surface taken on the same cleave surface as Fig. 2(a) without any intervening treatment of the sample and measured within hours of the image in Fig. 2(a). Notably, the surface on the right side of the image is filled with a dense network of domain walls, as seen in the pulse-induced mosaic phase previously described in TaS_2 [13,15,26]. Additionally, there appears to be a variation in intensity at or near the transition between the regular and mosaic regions of the image. This contrast is again strongly reminiscent of the pulse-induced mosaic phase; see, for example, Fig. 2 in Ref. [26].

In Fig. 2(c) we compare STS spectra obtained at three different points in Figs. 2(a) and 2(b) as marked by dots of the corresponding color. While the spectra taken at points on the nonmosaic part of the surface are gapped as expected for the CCDW phase, the blue spectrum taken within a domain of the mosaic region is metallic, as for the pulse-induced mosaic. Further STS measurements, presented in the Supplemental Material, obtained at different locations in Fig. 2(b) confirm that the visual contrast between the normal and mosaic phase consistently coincides with a change in the electronic behavior from insulating to metallic. To further verify whether this naturally occurring mosaic behaves the same electronically as the pulse-induced mosaic, Fig. 2(d) contains a cut across an STS map taken across the boundary between the normal and metallic mosaic phases which agrees very well with data previously obtained for the pulse-induced mosaic phase [26]. In particular, the shifting of the peak at −0.2 V towards the Fermi level and an accompanying shift of the gap into the unoccupied states is very similar to the pulse-induced mosaic phase.

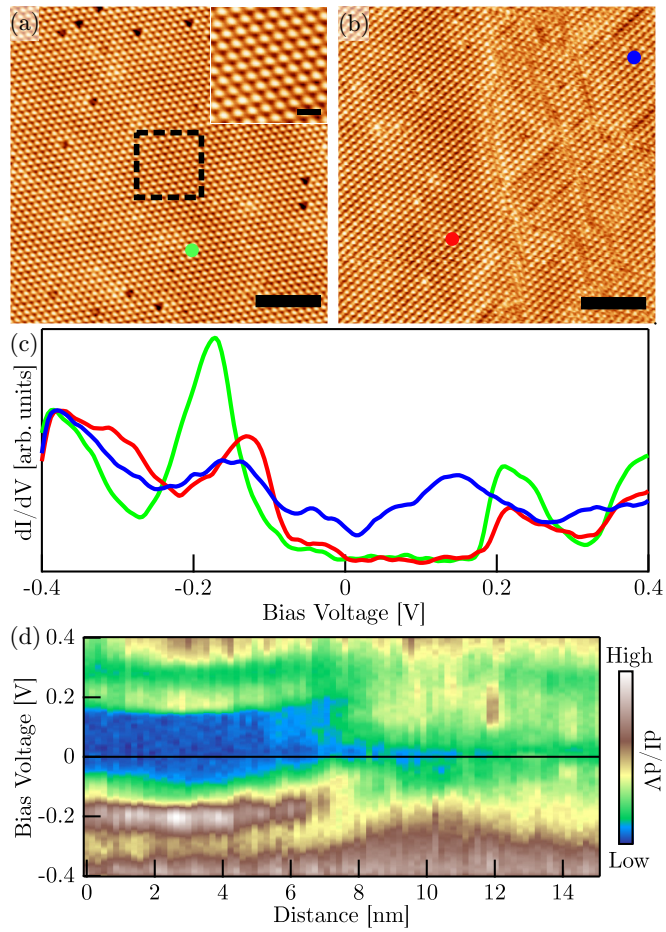

FIG. 2. (a) Typical STM image taken in the insulating CCDW phase of $1T$-TaS_2. Inset: an enlarged, defect free section of the main image marked by the dashed square therein. Note that the bright spots forming the lattice correspond to SODs, not individual atoms. The scale bar has a length of 10 nm for the main image and 4 nm for the inset. (b) STM image of a typical transition between the insulating CCDW phase on the left and the metallic mosaic phase on the right accompanied by a slight visual contrast. The image was taken at a different location on the same cleave as (a). The scale bar has a size of 10 nm. (c) Three STS spectra obtained at the points marked with the corresponding color in (a) and (b). The normal insulating behavior occurs in the nonmosaic parts of both images while the mosaic phase is metallic. (d) Cut across an STS map of a transition between insulating and metallic regions across a domain wall.

We will now focus on the immediate origins of the metallic behavior in the mosaic phase, starting from the hypothesis that a change of stacking of the top layer to AB stacking due to the presence of domain walls in only one of the top two layers is responsible for this metallicity. Using the assumption that the periodicity of the CDW in the second-to-top layer remains the same, that is to say, there is not coincidentally also a domain wall at the same location in the second-to-top layer, and knowing what stacking order is present in the normal insulating phase, one can reconstruct the stacking order in the metallic phase by extrapolating the lattice of one domain across the domain wall and comparing it to the lattice in a second domain. When then comparing the shift between the two lattices with the offsets between Ta atoms in the regular

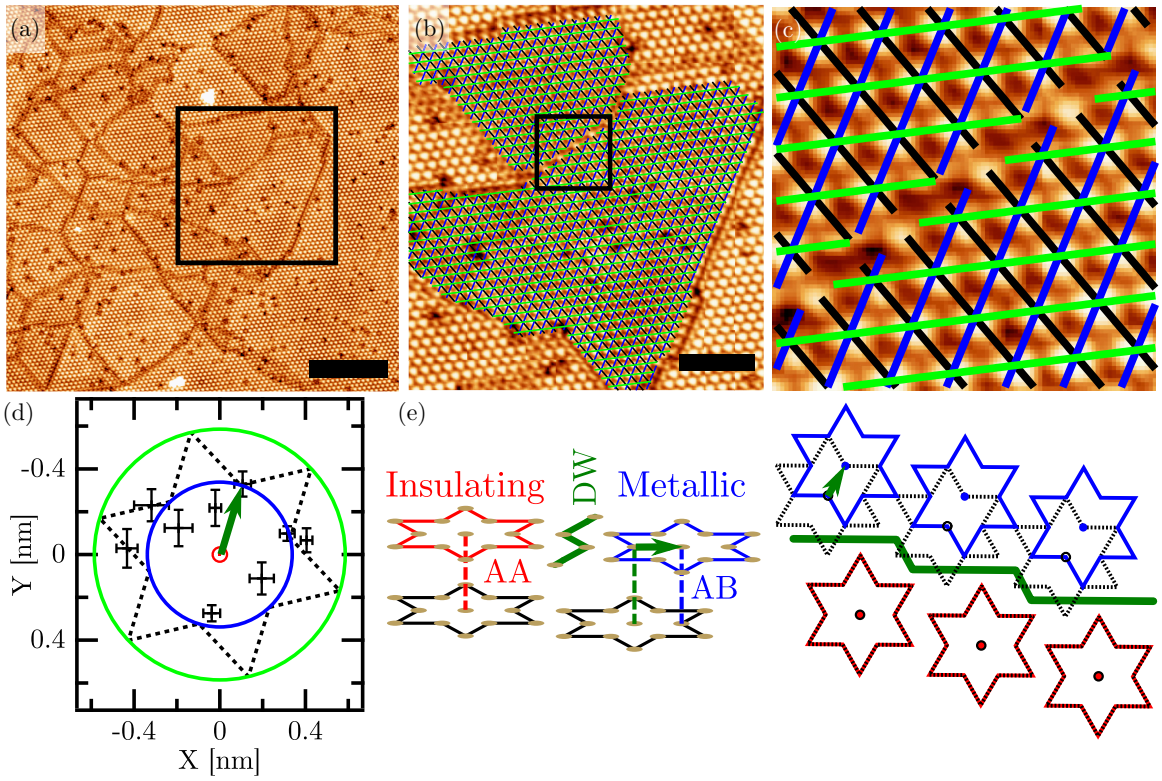

FIG. 3. (a) STM image of a region containing both metallic and insulating domains, as indicated by their differing intensities. The scale bar has a size of 20 nm. (b) Zoom on the region marked in (b) with lines fitted to SODs in two adjacent domains of different electronic character. The resulting crossing points align well with the SOD lattice. The scale bar has a size of 7 nm. (c) Further zoomed image on the domain wall between the two domains at the location marked in (c) with the same fitted lines. The shift of the SOD lattice between the two domains is visible by eye and most pronounced for the green and blue directions. The image has a total size of 7 × 7 nm. (d) The shifts of the top layer lattice between several pairs of domains with different electronic character overlaid on a schematic of a single SOD. The size of each cross indicates the uncertainty of the position. The blue and green circle represent the expected shift for AB and AC stacking, respectively. The dotted black star corresponds to one possible orientation of the CDW (see main text). The choice of rotation is made so as to be in better agreement with the individual shifts. (e) Schematic depiction of the proposed reason for the changes in stacking order. Left: the transition between insulating (red) and metallic (blue) phase across a top layer domain wall (DW) with the Ta atoms in the SOD drawn to illustrate the change in top layer stacking. The green arrow in the metallic (right) domain demonstrates the shift we calculate, as seen in (d). Right: view along the stacking direction with SODs in the insulating and metallic phases of the top layer in solid colors and the SODs of the second-to-top layer in dashed black. Note how the domain wall only occurs in the top layer, while the periodicity of the second-to-top layer continues uninterrupted. The green arrow in the metallic domain again corresponds to the shift we calculate.

atomic lattice, we can gain information about which shift has occurred across the domain wall and thus how the stacking changes. Further technical details of the analysis process can be found in the Supplemental Material.

We apply this method to the image in Fig. 3(a), which has several large domains with differing electronic character adjacent to each other, as seen from the visual contrast between the slightly darker metallic mosaic regions and the brighter insulating normal phase, which makes it suitable for our method of analysis. We assume that the normal phase in this image is AA stacked, due to the contrast between the insulating and metallic domains which is the same as in Fig. 2(b), which shows a large gap characteristic of this termination [24,29]. Additionally, we have also observed a metallic mosaic surrounded by an AC stacked normal phase, which shows a strikingly different contrast, as presented in the Supplemental Material. Figure 3(b) contains a zoom on two domains of different electronic character with fits applied along the three axes of the hexagonal CDW lattice represented by the colored lines. A further zoom onto the region around the domain wall is shown in Fig. 3(c). Here, the change of periodicity between the two domains can be seen by eye when comparing the lines along the same lattice directions on either side of the domain wall. Finally, the result of the analysis is presented in Fig. 3(d). The lattice shift between a total of nine sets of two adjacent domains each with different electronic character is indicated by the black crosses. In essence, the black crosses represent the center positions of the SODs of a metallic domain with respect to the center of the SODs in an adjacent insulating domain. The blue and green circles mark the distances of the inner Ta atoms of the SODs (corresponding to an AB stacking order) and outer Ta atoms (corresponding to AC stacking), respectively, while the red circled dot corresponds to AA stacking. The obtained shifts thus agree with the shift leading to an AB stacking in the metallic domains, providing support for a nonbulk stacking related origin of the metallicity of the mosaic phase only from knowledge about the top layer.

Figure 3(e) presents a schematic explanation of how this shift occurs. On the left, two layers of Ta atoms as well as the outline of the SOD CDW pattern can be seen. On the left side of the domain wall, the top layer is stacked in the AA configuration and thus displays the expected insulating behavior. However, on the transition across the domain wall in the top layer, the phase of the top layer CDW changes with respect to that of the second-to-top layer since the domain wall is composed of Ta atoms not participating in the formation of any complete SODs. Again, we assume here that no domain wall is occurring in the second-to-top layer at the same location. While domain walls in the second-to-top layer have been indirectly observed both in previous studies and in our own measurements [15,24,26], there is no reason to assume that they consistently occur in the same pattern as the ones in the top layer. As such, a spatial shift between the centers of the top and second-to-top layer CDW occurs, indicated by the green arrow, thus altering the stacking order. The right panel provides a top-down view of the same situation with the second-to-top layer SODs being indicated by dashed black lines. In the insulating phase on the bottom, the SODs overlap between the two layers whereas, in the metallic phase, the AB stacking order occurs due to the broken periodicity in the top layer caused by the domain wall, while the periodicity of the bottom layer CDW is maintained as no domain wall occurs in that layer. The shift which we have calculated for several domain walls in Fig. 3(d) is again represented by a green arrow in the top domain. Note that this same mechanism also allows for domain walls in the second-to-top layer, with no corresponding domain wall in the top layer, to change the stacking order within a single top layer domain. An example of this occurring can be seen just above and to the right of the center of Fig. 2(b), where a visual contrast and a change in electronic behavior occurs between the upper and lower parts of a single top layer domain.

We can further consider that the atomic lattice can only be aligned in two mirror symmetric ways relative to the CDW lattice. These two potential orientations of the atomic lattice are normally indistinguishable from knowledge of only the CDW lattice. However, as the structure of the CDW is not altered by lattice shifts, that is to say the shifted center of the SOD will nevertheless correspond to the location of a Ta atom, the obtained shifts should be located at the Ta locations of one of the two possible atomic lattices. From our analysis, we find that the shifts indeed align reasonably well with one potential atomic lattice as indicated by the dotted black star in Fig. 3(e). For reference, the second possible atomic lattice based on the CDW lattice would be rotated by 30° around the center of the SOD, meaning the atoms would be located on the same circles in Fig. 3(d) but centered between the atoms of the chosen lattice. This would correspond less well with our results. Therefore, our analysis is potentially capable of extracting information about the underlying *atomic* lattice from the behavior of the CDW across domain walls, even without an image with atomic resolution.

We stress here that this natural mosaic phase has been observed across numerous samples, cleaves, and macroscopically distinct locations on the surface of samples from different growth batches and produced by two different sources, each time accompanied by a closing of the electronic gap and a visual contrast between the two phases. We have also observed the mosaic phase after various periods of time after cleaving the sample, including in the very first measurement. Its appearance is therefore not likely to be related to sample ageing. Furthermore, while the metallic mosaic phase is sometimes confined to small areas of 10×10 nm^2, we also observe continuous mosaic regions extending over several hundreds of nanometers and covering a similar fraction of imaged surface area as the insulating normal phase. When selecting different measurement locations on the surface of the same sample we have also noted that, on multiple occasions, all measured locations within an area of $\sim$1 mm^2 on the sample surface contained a metallic mosaic, while other areas of the sample only showed the normal insulating phase. Additional STM and STS measurements demonstrating the above can be found in the Supplemental Material. Given this, we attribute the appearance of this phase in our samples to a sample-intrinsic property which occurs with some significant frequency across TaS_2 samples.

We now turn to the question of why this mosaic phase appears in our samples without the need for external stimulation, in contrast to previous studies. As mentioned above, the most immediately striking difference seen in our samples as compared to those in previous studies [15,24,26] is the larger amount of intrinsic defects in the CDW lattice, as seen for example in Fig. 3(a). To quantify this, we determined the number of defects in several STM images taken on samples which hosted the mosaic phase and found that an average of $2.9 \pm 0.4\%$ of surface SODs contained a defect in these images. In comparison, this value is over twice that of the highest density of such defects found in the existing literature [15,24,26]. Even more interestingly, recent investigations of Ti doped TaS_2 have also demonstrated the appearance of a metallic mosaic phase at low doping [29]. The density of Ti intercalation defects at the surface on which the mosaic phase is observed is 4.2% of surface SODs, similar to our results, though from the bulk doping of 1% one would expect 12% of SODs to show defects. Note that the highest density of surface defects in our measurements remains below the minimum doping reported in Ref. [29] for which only changes to the CCDW transition temperature and minor changes to the electronic structure are observed. This is further confirmed by the CCDW transition temperature in our samples which is the same as for pristine samples; see Fig. 1(d). Thus, in spite of the density of defects in our samples being higher than in previous studies, this does not impact the macroscopic properties of our samples. The defect density in our samples is also far removed from the doping level at which the insulating CDW phase is fully suppressed (8% Ti doping) [29,40], in agreement with our observations.

When considering the nature of the defects we observe, we first note that a large majority (>90%) of the defects we count in our images appear as a single darkened SOD at negative bias. We have obtained STS measurements on two different kinds of such defects which we present in the Supplemental Material. As a full taxonomy of native surface defects on TaS_2 is not available in the literature and is beyond the scope of this work, we cannot definitively identify the defects in our samples. We can still note certain similarities between the STS spectra we measure and those obtained at Ti substitution

[29] and S vacancy [41] sites. In contrast to these previous measurements, we do however only observe a partial closing of the gap for the defects in our samples. While we have no explanation for the potential presence of Ti atoms in our samples, it is possible that our growth method produced S vacancies, since we did not add sulfur beyond the stoichiometric ratio during the crystal growth as previously done in some cases [24,42] but not others [15]. We therefore tentatively suggest that the defects we principally find in our samples are sulfur vacancies, though this warrants further study.

One potential mechanism by which the increased number of defects could lead to the occurrence of the mosaic phase is the pinning of domain walls at defects sites during the cooling from the near commensurate CDW (NCCDW) phase to the CCDW phase. Though possible, the domain walls which exist in the NCCDW phase are qualitatively different from those in the CCDW phase and it is not obvious how one would directly turn into the other while pinned [43]. There is a different possible nonpinning related explanation for the relationship between defects and the mosaic phase based on theoretical work aimed at explaining the origin of the pulse-induced mosaic in TaS_2 [28]. From simulations, it was found that charged defects introduced into a hexagonal lattice lead to the formation of networks of charged, one-dimensional domain walls. This would be in line with our suggestion that the most commonly observed defect in our samples is a S vacancy which constitutes such a charged defect. Therefore, it appears plausible that the increased density of defects at the surface of our samples causes the formation of a dense network of domain walls, giving rise to the characteristic appearance of the mosaic phase in the same manner as for intentional doping of the sample [29]. The resulting high density of domain walls increases the probability of a domain wall occurring only in one of the top two layers, thus leading to the appearance of the metallic phase in the mosaic due to a change in stacking of the top layer as shown above. However, it is not clear why the majority of domains within the domain wall network would adopt this nonbulk stacking. It may be possible that instead the formation of domain walls due to the effects of intrinsic defects upon cooling is favored within regions of altered stacking. These findings also provide insight into a potential mechanism of the creation of the pulse-induced mosaic phase, namely that the pulses create similar charged defects in the CDW lattice, which then cause the formation of domain walls as the lattice cools again [14].

IV. CONCLUSION

In conclusion, we have shown the occurrence of a metallic mosaic phase at the surface of 1*T*-TaS_2 without the need for external stimulation through laser or electrical pulses. Our characterization of this phase reveals that it behaves the same as the pulse-induced phase, leading us to assume that they are the same and opening up the possibilities for study of this phase without the need for additional preparation steps. In analogy with the behavior of Ti doped TaS_2 samples and supported by previous model calculations, we suggest that the origin of the mosaic phase in our samples is found in a higher density of charged surface defects which lead to the formation of a network of domain walls. We have tentatively identified these defects as S vacancies. Through further analysis of our measurements, we have demonstrated how interlayer stacking could plausibly be changed within the metallic surface domains due to the occurrence of domain walls in only one of the two top layers, which is made more likely by the presence of a large number of domain walls in the mosaic phase. This mechanism can also serve as an explanation for the pulse-induced mosaic phase if one assumes that localized charged defects are created in the CDW lattice by the pulses.

ACKNOWLEDGMENT

B.S. and C.M. acknowledge support from the Swiss National Science Foundation Grant No. P00P2_170597.

[1] K. S. Novoselov, A. K. Geim, S. V. Morozov, D. Jiang, Y. Zhang, S. V. Dubonos, I. V. Grigorieva, and A. A. Firsov, Electric field effect in atomically thin carbon films, Science **306**, 666 (2004).

[2] L. Li, Y. Yu, G. J. Ye, Q. Ge, X. Ou, H. Wu, D. Feng, X. H. Chen, and Y. Zhang, Black phosphorus field-effect transistors, Nat. Nanotechnol. **9**, 372 (2014).

[3] Y. Chen, Y. Sun, J. Peng, J. Tang, K. Zheng, and Z. Liang, 2D Ruddlesden-Popper perovskites for optoelectronics, Adv. Mater. **30**, 1703487 (2018).

[4] J. Yan, W. Qiu, G. Wu, P. Heremans, and H. Chen, Recent progress in 2D/quasi-2D layered metal halide perovskites for solar cells, J. Mater. Chem. A **6**, 11063 (2018).

[5] X. Zhou, X. Hu, S. Zhou, H. Song, Q. Zhang, L. Pi, L. Li, H. Li, J. Lü, and T. Zhai, Tunneling diode based on WSe_2/SnS_2 heterostructure incorporating high detectivity and responsivity, Adv. Mater. **30**, 1703286 (2018).

[6] Q. H. Wang, K. Kalantar-Zadeh, A. Kis, J. N. Coleman, and M. S. Strano, Electronics and optoelectronics of two-dimensional transition metal dichalcogenides, Nat. Nanotechnol. **7**, 699 (2012).

[7] D. H. Keum, S. Cho, J. H. Kim, D.-H. Choe, H.-J. Sung, M. Kan, H. Kang, J.-Y. Hwang, S. W. Kim, H. Yang *et al.*, Bandgap opening in few-layered monoclinic $MoTe_2$, Nat. Phys. **11**, 482 (2015).

[8] G. Wang, L. Li, W. Fan, R. Wang, S. Zhou, J.-T. Lü, L. Gan, and T. Zhai, Interlayer coupling induced infrared response in WS_2/MoS_2 heterostructures enhanced by surface plasmon resonance, Adv. Funct. Mater. **28**, 1800339 (2018).

[9] S. Bhattacharyya and A. K. Singh, Semiconductor-metal transition in semiconducting bilayer sheets of transition-metal dichalcogenides, Phys. Rev. B **86**, 075454 (2012).

[10] J. Hong, C. Wang, H. Liu, X. Ren, J. Chen, G. Wang, J. Jia, M. Xie, C. Jin, W. Ji *et al.*, Inversion domain boundary induced stacking and bandstructure diversity in bilayer $MoSe_2$, Nano Lett. **17**, 6653 (2017).

[11] X. L. Wu and C. M. Lieber, Hexagonal domain-like charge density wave phase of TaS_2 determined by scanning tunneling microscopy, Science **243**, 1703 (1989).

[12] C. Scruby, P. Williams, and G. Parry, The role of charge density waves in structural transformations of 1T-TaS_2, Philos. Mag. **31**, 255 (1975).

[13] L. Stojchevska, I. Vaskivskyi, T. Mertelj, P. Kusar, D. Svetin, S. Brazovskii, and D. Mihailovic, Ultrafast switching to a stable hidden topologically protected quantum state in an electronic crystal, Science **344**, 177 (2014).

[14] Q. Stahl, M. Kusch, F. Heinsch, G. Garbarino, N. Kretzschmar, K. Hanff, K. Rossnagel, J. Geck, and T. Ritschel, Collapse of layer dimerization in the photo-induced hidden state of $1T$-TaS_2, Nat. Commun. **11**, 1247 (2020).

[15] D. Cho, S. Cheon, K.-S. Kim, S.-H. Lee, Y.-H. Cho, S.-W. Cheong, and H. W. Yeom, Nanoscale manipulation of the Mott insulating state coupled to charge order in $1T$-TaS_2, Nat. Commun. **7**, 10453 (2016).

[16] M. J. Hollander, Y. Liu, W.-J. Lu, L.-J. Li, Y.-P. Sun, J. A. Robinson, and S. Datta, Electrically driven reversible insulator–metal phase transition in $1T$-TaS_2, Nano Lett. **15**, 1861 (2015).

[17] I. Vaskivskyi, I. Mihailovic, S. Brazovskii, J. Gospodaric, T. Mertelj, D. Svetin, P. Sutar, and D. Mihailovic, Fast electronic resistance switching involving hidden charge density wave states, Nat. Commun. **7**, 1 (2016).

[18] J. Ravnik, M. Diego, Y. Gerasimenko, Y. Vaskivskyi, I. Vaskivskyi, T. Mertelj, J. Vodeb, and D. Mihailovic, A time-domain phase diagram of metastable states in a charge ordered quantum material, Nat. Commun. **12**, 2323 (2021).

[19] Z. Wu, K. Bu, W. Zhang, Y. Fei, Y. Zheng, J. Gao, X. Luo, Z. Liu, Y.-P. Sun, and Y. Yin, Effect of stacking order on the electronic state of $1T$-TaS_2, Phys. Rev. B **105**, 035109 (2022).

[20] C. W. Nicholson, F. Petocchi, B. Salzmann, C. Witteveen, M. Rumo, G. Kremer, F. O. von Rohr, P. Werner, and C. Monney, Modified interlayer stacking and insulator to correlated-metal transition driven by uniaxial strain in $1T$-TaS_2, arXiv:2204.05598.

[21] T. Endo, S. Nakao, W. Yamaguchi, T. Hasegawa, and K. Kitazawa, Influence of CDW stacking disorder on metal–insulator transition in $1T$-TaS_2, Solid State Commun. **116**, 47 (2000).

[22] R. Hovden, A. W. Tsen, P. Liu, B. H. Savitzky, I. El Baggari, Y. Liu, W. Lu, Y. Sun, P. Kim, A. N. Pasupathy *et al.*, Atomic lattice disorder in charge-density-wave phases of exfoliated dichalcogenides ($1T$-TaS_2), Proc. Natl. Acad. Sci. USA **113**, 11420 (2016).

[23] T. Ritschel, H. Berger, and J. Geck, Stacking-driven gap formation in layered $1T$-TaS_2, Phys. Rev. B **98**, 195134 (2018).

[24] C. Butler, M. Yoshida, T. Hanaguri, and Y. Iwasa, Mottness versus unit-cell doubling as the driver of the insulating state in $1T$-TaS_2, Nat. Commun. **11**, 2477 (2020).

[25] F. Petocchi, C. W. Nicholson, B. Salzmann, D. Pasquier, O. V. Yazyev, C. Monney, and P. Werner, Mott versus Hybridization Gap in the Low-Temperature Phase of $1T$-TaS_2, Phys. Rev. Lett. **129**, 016402 (2022).

[26] L. Ma, C. Ye, Y. Yu, X. F. Lu, X. Niu, S. Kim, D. Feng, D. Tománek, Y.-W. Son, X. H. Chen *et al.*, A metallic mosaic phase and the origin of Mott-insulating state in $1T$-TaS_2, Nat. Commun. **7**, 10956 (2016).

[27] Y. Wang, W. Yao, Z. Xin, T. Han, Z. Wang, L. Chen, C. Cai, Y. Li, and Y. Zhang, Band insulator to Mott insulator transition in $1T$-TaS_2, Nat. Commun. **11**, 4215 (2020).

[28] P. Karpov and S. Brazovskii, Modeling of networks and globules of charged domain walls observed in pump and pulse induced states, Sci. Rep. **8**, 4043 (2018).

[29] W. Zhang, J. Gao, L. Cheng, K. Bu, Z. Wu, Y. Fei, Y. Zheng, L. Wang, F. Li, X. Luo *et al.*, Visualizing the evolution from Mott insulator to Anderson insulator in Ti-doped $1T$-TaS_2, npj Quantum Mater. **7**, 8 (2022).

[30] L. Perfetti, T. A. Gloor, F. Mila, H. Berger, and M. Grioni, Unexpected periodicity in the quasi-two-dimensional Mott insulator $1T$-TaS_2 revealed by angle-resolved photoemission, Phys. Rev. B **71**, 153101 (2005).

[31] A. S. Ngankeu, S. K. Mahatha, K. Guilloy, M. Bianchi, C. E. Sanders, K. Hanff, K. Rossnagel, J. A. Miwa, C. Breth Nielsen, M. Bremholm, and P. Hofmann, Quasi-one-dimensional metallic band dispersion in the commensurate charge density wave of $1T$-TaS_2, Phys. Rev. B **96**, 195147 (2017).

[32] B. Sipos, A. F. Kusmartseva, A. Akrap, H. Berger, L. Forró, and E. Tutiš, From Mott state to superconductivity in $1T$-TaS_2, Nat. Mater. **7**, 960 (2008).

[33] H. P. Hughes and J. A. Scarfe, Site Specific Photohole Screening in a Charge Density Wave, Phys. Rev. Lett. **74**, 3069 (1995).

[34] S. Hellmann, M. Beye, C. Sohrt, T. Rohwer, F. Sorgenfrei, H. Redlin, M. Kalläne, M. Marczynski-Bühlow, F. Hennies, M. Bauer *et al.*, Ultrafast Melting of a Charge-Density Wave in the Mott Insulator $1T$-TaS_2, Phys. Rev. Lett. **105**, 187401 (2010).

[35] See Supplemental Material at http://link.aps.org/supplemental/10.1103/PhysRevMaterials.7.064005 for additional characterization measurements and details of the analysis process.

[36] E. Hujala, V. Tanskanen, and J. Hyvärinen, Pattern recognition algorithm for analysis of chugging direct contact condensation, Nucl. Eng. Des. **332**, 202 (2018).

[37] G. Patel, E. Hujala, M. Puustinen, and J. Hyvärinen, Modeling of horizontal steam injection in a water pool, Nucl. Eng. Design **405**, 112197 (2023).

[38] MATLAB, *version 9.8 (R2020a)*, The MathWorks Inc., Natick, Massachusetts, USA, 2020.

[39] N. Otsu, A threshold selection method from gray-level histograms, IEEE Trans. Syst., Man, Cybernet. **9**, 62 (1979).

[40] J. Gao, W. Zhang, J. Si, X. Luo, J. Yan, Z. Jiang, W. Wang, H. Lv, P. Tong, W. Song *et al.*, Chiral charge density waves induced by Ti-doping in $1T$-TaS_2, Appl. Phys. Lett. **118**, 213105 (2021).

[41] I. Lutsyk, K. Szalowski, P. Krukowski, P. Dabrowski, M. Rogala, W. Kozlowski, M. L. Ster, M. Piskorski, D. Kowalczyk, W. Rys *et al.*, Influence of structural defects on charge density waves in $1T$-TaS_2, Nano Res. (2023), doi:10.1007/s12274-023-5876-7.

[42] R. Inada and S.-i. Tanuma, Anderson localization and crystalline defects of $1T$-TaS_2, J. Phys. Soc. Jpn. **52**, 3536 (1983).

[43] J. W. Park, G. Y. Cho, J. Lee, and H. W. Yeom, Emergent honeycomb network of topological excitations in correlated charge density wave, Nat. Commun. **10**, 4038 (2019).